Supporting Information

Singh et al. 10.1073/pnas.1119416110

SI Materials and Methods

Cell Transplantation. Host mice were either C3H/HeNHsd (*rd1*) (Harlan) or Tg(CAG-DsRed*MST)1Nagy/J, aged 10–12 wk. Hosts were anesthetized with an i.p. injection of medetomidine hydrochloride (1 mg/kg body weight) and ketamine (60 mg/kg body weight) in sterile water in the ratio of 5:3:42. Pupils were dilated using 1% (wt/vol) tropicamide (Bausch & Lomb) to facilitate transpupillary visualization with an operating microscope (Leica). Cells were transplanted subretinally using a Hamilton syringe and a sharp 34-gauge needle inserted tangentially through the sclera into the subretinal space, creating a long self-sealing scleral tunnel. Under direct vision, the entire bevel was placed within the subretinal space to avoid reflux. The cell suspension was injected, creating a consistently sized superotemporal bleb. To further minimize expulsion of transplanted cells, normalization of intraocular pressure was verified by continuous direct ophthalmoscopy to monitor for the full return of retinal vessel perfusion, optic nerve head perfusion, and corneal clarity before rapid needle withdrawal.

Scanning Laser Ophthalmoscopy. Imaging was performed with Spectralis HRA (Heidelberg Engineering). The near-infrared reflectance mode (820-nm laser) was used for camera alignment. Fluorescence was excited using a laser diode centered at 488 nm, and emission was recorded between 500 and 700 nm. The 55° lens was used and images recorded at 4.6 frames/s.

Tissue Collection. Mice were perfusion fixed with 1–4% paraformaldehyde (PFA) in PBS. Retinal sections were prepared by cryoprotecting fixed eyes in 20% (wt/vol) sucrose before embedding in optimum cutting temperature compound (TissueTek) and frozen in isopentane cooled in liquid nitrogen. Cryosections (16–18 μm) were cut and affixed to poly-L-lysine–coated slides. For flat mounts, retinas were dissected free in PBS or collected after calcium imaging and fixed in 4% (wt/vol) PFA overnight.

Histology and Immunohistochemistry. Retinal sections or flat mounts were blocked in 0.01 M PBS containing serum and 0.1% Triton-X 100 for 1–3 h before being incubated with primary antibody overnight (flat mounts: 3 d) at 4 °C. After rinsing 3 × 5 min with PBS, sections were incubated with 1:400 appropriate Alexa-tagged secondary antibodies (Molecular Probes, Invitrogen) for 2 h at 4 °C, rinsed, and counterstained with Hoechst 33342. Specimens were mounted using ProLong Gold (Invitrogen). Primary antibodies are listed in Table S1.

Confocal Microscopy. Retinal sections were viewed on a confocal microscope (Zeiss LSM710). GFP-positive cells were located using epifluorescence illumination before taking a series of XY optical sections. The fluorescence of Hoechst, GFP, DsRed, Alexa-555, Alexa-568, and Alexa-635 was sequentially excited using 350-nm UV, 488-nm argon, and the 543-nm HeNe lasers, as appropriate. Stacks were built to give XY projection images where appropriate, and images were processed using Volocity (Perkin-Elmer), Image J, and Adobe Photoshop CS4 version 11.0.2.

Histological Analyses. For rod outer segment (OS) position assessment, confocal microcopy images were obtained of non-overlapping transplant regions of equal size, and Pde6b-positive OS in the inner, middle, and outer nuclear layer (ONL) were counted manually. Assessment of long/medium wave (LM) opsin in host retinal sections was done by obtaining confocal microscopy images through the portion of peripheral retina containing the most surviving cones and by quantifying LM opsin by standardized threshold detection using Image J (developed by Wayne Rasband, National Institutes of Health; available at http://rsb.info.nih.gov/ij/index.html).

Pupillometry. Following dark adaptation for >8 h, during the light phase of the mouse light-dark cycle, unanesthetized mice were held with the right (unoperated) eye facing an infrared camera. The left (operated) eye was subjected to a 100-ms duration white light through a light guide from a 100-W xenon arc lamp (LOT-Oriel) via a Ganzfeld sphere to ensure reproducible and directionally independent full field retinal illumination. Stimuli were presented in ascending irradiance controlled by neutral density filters, with completion of recordings at one intensity at a time for all animals. Animals were left unrestrained in complete darkness for >30 min between exposures in each eye. Pupil area was measured 1.9 s after stimulus offset (a_i) (this latency was consistently on the downslope of the initial fast phase of the pupil constriction curve) and was normalized to prestimulus pupil area (a_0) for comparisons between individuals. In each group, pupillometry curves were generated before and 2 wk after transplantation following the identical protocol.

mRNA Expression Analysis. Postnatal day 2–3 (P2–3) Tg(*Nrl-L-EGFP*) cells were injected subretinally ($n = 7$) or intravitreally ($n = 6$) into *rd1* hosts or maintained in vitro ($n = 5$ wells) with supplemented DMEM and were exposed to each niche condition for 14 d. We used adult (>6 wk, $n = 8$) and P16 ($n = 8$) Tg(*Nrl-L-EGFP*) animals to determine gene expression levels in mature rods. RNA was isolated from wells or whole eyes with extraction reagent (TRIzol; Gibco) and purified (RNeasy; Qiagen). cDNA was synthesized using the qScript cDNA Synthesis Kit (Quanta Biosciences). Quantitative real-time PCR was performed on Applied Biosystems 7500 Real-Time PCR System using SYBR Green PCR Master Mix. Gene amplification data were analyzed using Applied Biosystems 7500 System Sequence Detection Software version 1.2.3. For analysis of the effect of niche, the levels of *Nrl* and *Gfp* expression were used to control for the number of Tg(*Nrl-L-EGFP*) cells in each condition. Results were expressed as *n*-fold change in expression relative to P0 retinae ($n = 7$), using the ΔΔCT method. For analysis of effect of treatment versus sham, *Arp*, *Gapdh*, *B2-m*, and *Psmb2* were used as housekeeping genes, and the data were normalized to expression in *rd1* eyes ($n = 7$). Primer sequences are shown in Table S2.

Electroretinography. Full-field scotopic electroretinograms were obtained from parent and progeny of the Tg(CAG-DsRed*MST)1Nagy/J outcross to wild-type and *rd1* animals. Animals were dark-adapted overnight (>12 h) before testing. Anesthetized mice were placed on a heated stage, and silver thread DTL-type electrodes were placed on the eyes with custom contact lenses. Ground and reference electrodes were placed in the flank and scruff, and responses to 0.01 cd·sm^{-2} and 10 cd·sm^{-2} white light stimuli were recorded at a 5-kHz digitization rate for both eyes using the Espion system (Diagnosys). Unfiltered responses were analyzed offline.

Calcium Imaging. Neural retinas transplanted with P3 Tg(*Nrl-L-EGFP*) cells were dissected free in ice-cold Ringer's solution containing (in mM) 119 NaCl, 2.5 KCl, 1 KH_2PO_4, 1.3 $MgCl_2$, 2.5 $CaCl_2$, 26.2 $NaHCO_3$, and 11 D-glucose, equilibrated with 95% O_2/5% CO_2 (pH 7.4). Retinas were transferred photore-

ceptor side-up to the stage of an upright microscope (Olympus BX), held flat under a nylon-strung platinum wire harp, loaded with 10 μM Fura 2-AM (Molecular Probes) in Ringer's solution (0.5% DMSO; 0.1% pluronic acid dispersant) for 1.5 h at 30 °C, and then washed in Ringer's solution for 30 min for de-esterification. The indicator was excited alternately at 340 and 380 nm via a monochromator (Cairn Research Ltd) at 400 and 250 ms of exposure, respectively. Emission (510 nm) was captured with an intensified CCD camera (IPentamax, Princeton Instruments) every 2 s, and ratio images were generated (Metafluor, Universal Imaging). Drugs were applied by micropipette injection into the bathing solution. DCPG [(S)-3,4-dicarboxyphenylglycine, 20 μM final concentration in bath] and CPPG [(RS)-α-cyclopropyl-4-phosphonophenylglycine, 100 μM] were supplied by Tocris.

Light-Mediated Behavior Assay. Using a light-chamber/dark-chamber apparatus, the general principles of which have been described (1), preference for light or dark was assayed in female *rd1* mice aged ∼12 wk that had received bilateral P3 rod precursor transplants ($n = 7$) or bilateral sham rodless transplants ($n = 8$) and ∼10-wk-old control *rd1* mice that had received no transplant ($n = 8$). Mice were tested in a custom-made arena measuring 26 × 26 × 26 cm containing equally sized dark and light chambers connected by a 4- × 5-cm aperture at midpoint. The assay was modified to assess rod-mediated function: mice were dark adapted >12 h before testing, testing was conducted in a dark room, and the light chamber was lit by a custom LED array suspended above the chamber emitting dim green light centered at 510 nm (a longer wavelength than the peak of melanospin sensitivity and close to the rhodopsin peak) providing a maximal illumination of 150 $nW{\cdot}cm^{-2}{\cdot}s^{-1}$ or ∼10 lx. Both chambers had removable tops to allow thorough cleaning with 70% (vol/vol) ethanol before each test. Both pupils were dilated with one drop of 1% (wt/vol) atropine instilled ∼10 min before testing. Under dim red light, each mouse was placed in the tester's palm, ensuring minimal tail restraint, and gently placed in the middle of the chamber to be lit (front half), facing away from the connecting aperture. The tester was masked to treatment group. The chambers were closed, LED light was turned on, and video recording commenced. Each trial lasted 10 min, and all mice were test-naive (one trial per mouse). A mouse was deemed to have entered a chamber when four paws had crossed into that chamber. Mice were assayed for time spent in the lit chamber and for the number of full-body transitions between chambers (measure of anxiety-related behavior); data were calculated manually by viewing the video recording. One mouse was excluded from analysis due to nonexploration (0 transitions). Mean wild-type (WT) time in light was derived by testing non-*rd1* controls of the same background strain ($n = 5$).

Laser Speckle Cortical Imaging. Cortices were imaged of female *rd1* mice aged ∼12 wk that had received P3 rod precursor transplants in both eyes ($n = 7$) with $\sim 3 \times 10^5$ transplanted cells per eye. The positive control group consisted of mice from the same background strain but were *wt* rather than *rd1* at the *Pde6b* locus (WT, $n = 5$). As a negative control, we used *rd1* mice that had undergone equivalent bilateral sham rodless transplants from *rd1* donors ($n = 7$) to control for any possible effects of surgery and non-rod-cell transplantation on visual cortex blood flow (CBF). Mice were dark adapted >12 h, and testing was conducted in a dark room. Mice were anesthetized with an i.p. injection of medetomidine hydrochloride (1 mg/kg body weight) and ketamine (60 mg/kg body weight), and both eyes were dilated with tropicamide 1% (wt/vol) and phenylephrine 2.5% (wt/vol) (Bausch & Lomb). The head was fixed in a stereotaxic frame, and the scalp was incised to reveal the cranium over the visual cortices. Transcranial imaging was performed using the Speckle Contrast Imager (moorFLPI, Moor Instruments). Both eyes were simultaneously stimulated by brief flashes of light (∼10 μs) at 4 Hz for 1 s (Grass PS33 photic stimulator with flash lamp). A 1-min interstimulus interval was used with between 9 and 11 stimulus repeats for each animal. Data were processed using moorFLPI Review software and analyzed with MATLAB R2012a (7.14.0.739) and Origin Pro-8.6. Percentage changes in CBF were calculated relative to prestimulus baseline measurements, and trial-averaged CBF changes were computed for left and right visual cortices in each mouse. Control Fig. 4*K* was obtained with left-eye stimulation in a WT animal.

Statistical Analyses. OS position and pupillometry results were analyzed using paired two-tailed Student *t* tests (with Bonferroni correction where appropriate). Calcium imaging data were analyzed using paired or unpaired (as appropriate) two-tailed Student *t* tests. Quantitative PCR and relative pupil constriction amplitude data were analyzed using one-way ANOVA and Games–Howell post hoc or Mann–Whitney *U* test as appropriate. Pupillometry groups at baseline were compared using the Kruskal–Wallis test. Light-mediated behavior and cortical imaging data were compared using one-way ANOVA (Gabriel post hoc for light-mediated behavior and Dunnett *t* post hoc for cortical imaging). LM opsin data were analyzed using two-tailed Student *t* test. $\alpha = 0.05$ for all tests. Statistical analyses were carried out using SPSS version 19 (IBM), and charts were prepared using Graphpad Prism 5 for Mac version 5.0d or Origin Pro-8.6.

1. Semo M, et al. (2010) Dissecting a role for melanopsin in behavioural light aversion reveals a response independent of conventional photoreception. *PLoS ONE* 5(11): e15009. doi:10.1371/journal.pone.0015009.

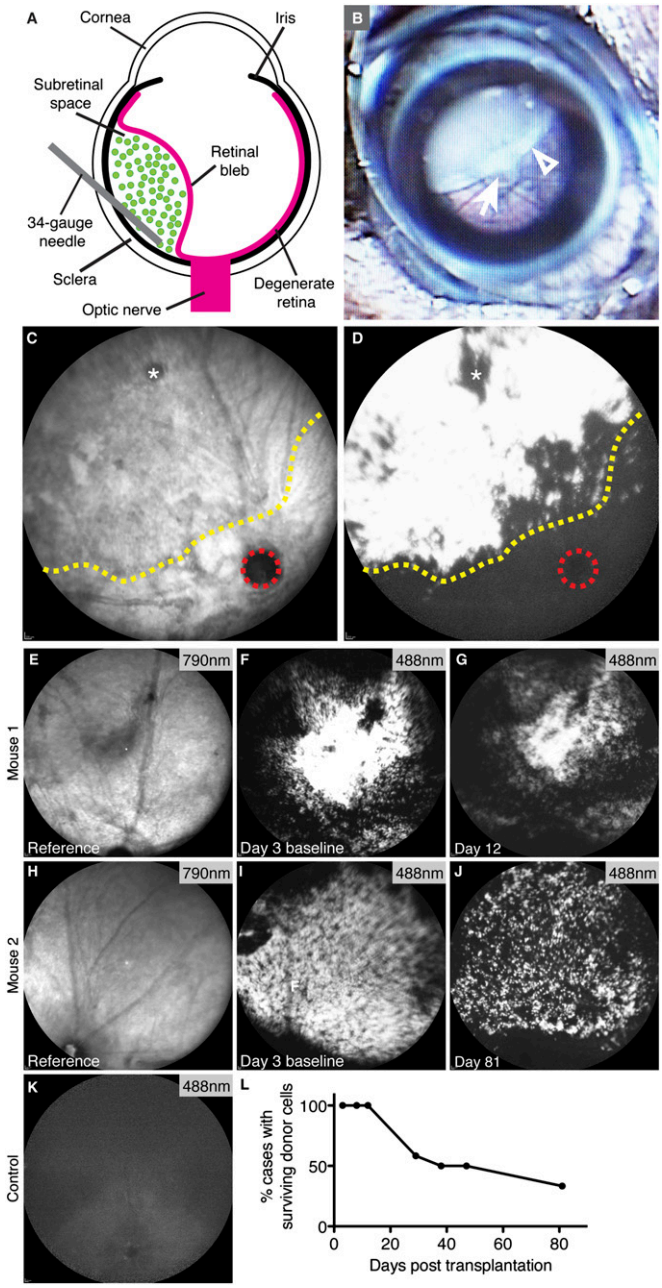

Fig. S1. (*A*) Standardized and reproducible cell delivery is feasible in end-stage degenerate hosts. The diagram illustrates subretinal transplantation of cells (green circles) using a long, oblique 34-gauge scleral tunnel that minimized reflux of transplanted cells out of the eye. The lens has been omitted for clarity. (*B*) Intraoperative transpupillary view in a representative case, showing the surface extent of the retinal bleb (arrowhead) raised by the subretinal suspension. The optic nerve head (arrow) is clearly seen. Thirty to forty percent retinal coverage was ensured at the end of the transplantation in every case ($n = 12$, precursor transplantation; $n = 11$, sham), along with absence of complications such as bleeding or perforation. (*C* and *D*) To confirm the presence of viable donor cells before functional analysis at 2 wk, we used in vivo confocal scanning laser ophthalmoscopy to obtain 820-nm near-infrared reflectance (*C*) and 488-nm autofluorescence (*D*) images to detect and localize green fluorescent donor-derived cells (white signal in *D*). The posterior extent of the grafts (dashed yellow line) could be judged by comparison with the location of the optic nerve head (dashed red circle). Asterisks in *C* and *D* show the scleral penetration site. (*E*–*L*) Long-term outcomes following subretinal transplantation of precursor cells into adult mice, which had no preexisting outer nuclear layer. (*E*–*G*) In vivo reference and fluorescence images from a recipient eye in which the transplanted cells, which emit fluorescence at 488 nm, were seen to survive up to day 12. (*H*–*J*) In another mouse, transplanted cells were seen to survive up to the last assessment time point at 81 d. (*K*) A control 488-nm fluorescence image of a degenerate eye without donor cells. (*L*) Time course showing percentage of eyes ($n = 12$) with surviving donor cells after transplantation.

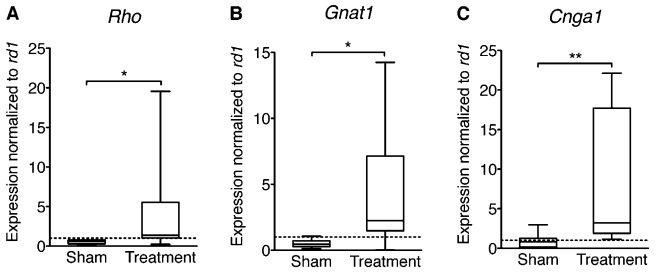

Fig. S2. Outer retinal reconstruction with precursor cells restored the expression of (*A*) *Rho*, (*B*) *Gnat1*, and (*C*) *Cnga1* in *rd1* eyes, compared with sham treatment. *Rho* ($U_1 = 9$, $Z = -2.54$, $P = 0.01$), *Gnat1* ($U_1 = 10$, $Z = -2.44$, $P = 0.014$), and *Cnga1* ($U_1 = 5$, $Z = -2.93$, $P = 0.002$). $^*P < 0.05$, $^{**}P < 0.01$, $n = 10$ (sham), $n = 7$ (treatment). Whiskers indicate range of values, and dashed line indicates normalized expression of 1.

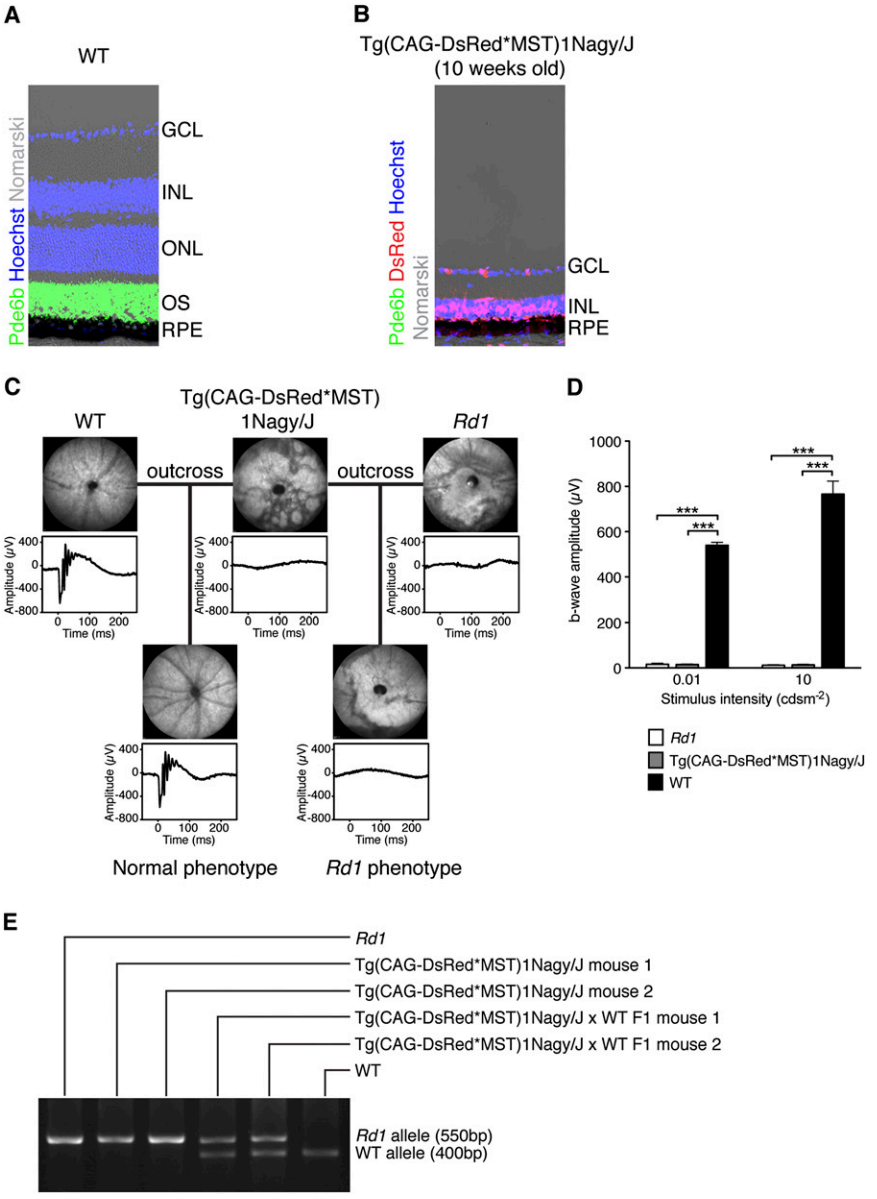

Fig. S3. Characterization of the severe retinal degeneration phenotype in the Tg(CAG-DsRed*MST)1Nagy/J hosts. (*A*) WT retina showing thee nuclear layers in the normal thick retina and strong immunostaining for cGMP phosphodiesterase β6 (Pde6b) in OS. (*B*) In 10-wk-old Tg(CAG-DsRed*MST)1Nagy/J host mice, the outer retina is severely degenerate and there is no immunoreactivity to Pde6b. (*C*) Outcross data confirm the *rd1* genotype in Tg(CAG-DsRed*MST)1Nagy/J mice. (*D*) The b-wave electroretinogram amplitude is severely reduced in Tg(CAG-DsRed*MST)1Nagy/J host mice, similar to that in *rd1* mice, compared with WT controls at low ($F_{2,12} = 1{,}445.17$, $P = 5.0 \times 10^{-15}$, $^{***}P < 0.001$ post hoc, $n = 5$ in each group) and high ($F_{2,12} = 170.14$, $P = 1.6 \times 10^{-9}$, $^{***}P < 0.001$ post hoc, $n = 5$ in each group) stimulus intensities. (*E*) Duplex PCR for the *Pde6b*^{rd1} allele shows that Tg(CAG-DsRed*MST)1Nagy/J mice are homozygous for the *Pde6b*^{rd1} mutation. GCL, ganglion cell layer. INL, inner nuclear layer. ONL, outer nuclear layer. RPE, retinal pigment epithelium.

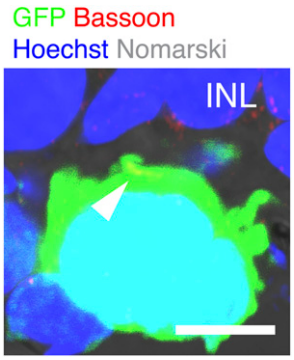

Fig. S4. Donor-derived rods express bassoon in the perinuclear cytoplasm. In contrast to other reports where a host outer nuclear layer exists before transplantation of donor cells, in the totally degenerate retina, no photoreceptor inner fiber was seen (the elongated cytoplasmic process that connects the rod perinuclear cytoplasm proximally to the rod spherule synapse). To explore the anatomy of the synapse further, we used immunostaining for bassoon, an essential component of the ribbon synapse. The punctate pattern of expression was clearly visible and showed that ribbon synapses were forming within the perinuclear cytoplasm (arrowhead), confirming, with the synaptophysin staining described in the text, that transplanted cells in the totally degenerate host adopt a different morphology from normal photoreceptors. The host inner nuclear layer (INL) is shown. (Scale bar, 5 μm.)

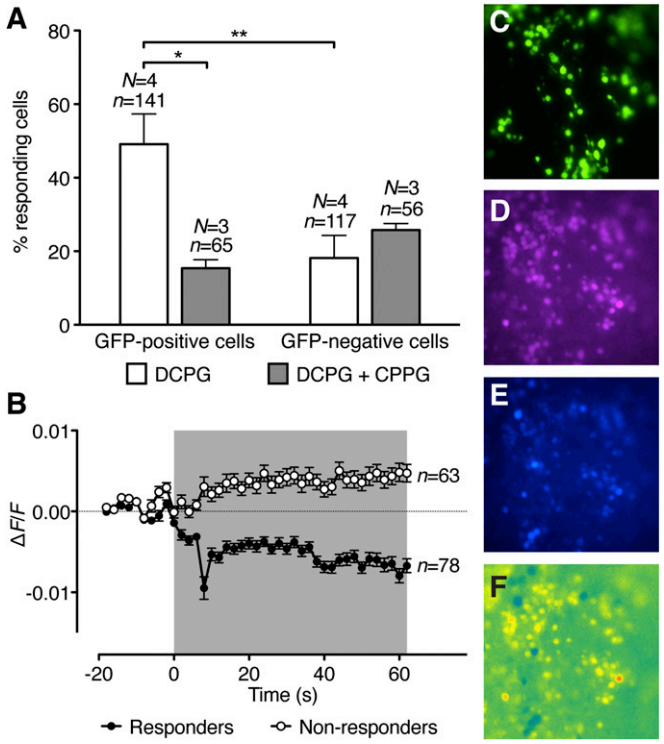

Fig. S5. Transplanted donor rod responses to a glutamate receptor agonist–antagonist pair shows a rod-specific pattern of intracellular calcium concentration change. We used calcium imaging to examine integrated green fluorescent protein (GFP)-positive donor cells in posttransplantation retinal explants. Non-GFP–expressing cells in the same explants acted as internal controls. (*A*) Addition of the specific mGluR8 agonist, (S)-3,4-dicarboxyphenylglycine (DCPG), resulted in an expected decrease in intracellular calcium concentration in 49.1 ± 8.2% of GFP-positive (donor) cells vs. 18.2 ± 6.1% of controls (**$t_3 = 9.09$, $P = 0.003$, $n = 4$). The response was blocked by the specific antagonist (RS)-a-cyclopropyl-4-phosphonophenylglycine (CPPG), confirming an earlier report (1) (*$t_{3.46} = 3.94$, $P = 0.02$, $N_1 = 4$, $N_2 = 3$). This not only confirmed the identity of the GFP-positive cells as mature rods, but also indicated that many of the cells had differentiated sufficiently to contain the homeostatic apparatus for calcium autoregulation critical to their function. (*B*) Averaged traces of the change in fluorescence intensity in 141 GFP-positive cells in response to DCPG stimulation, showing a clear difference between responding and nonresponding cells. Representative fluorescence images obtained with stimulation at 488 nm (*C*), 340 nm (*D*), and 380 nm (*E*), enabling the selection of GFP-positive and -negative cells for analysis. (*F*) Colorimetric representation of the ratio between 340- and 380-nm fluorescence in the same retinal explant. Data are mean ± SE of mean. *N*, number of retinas; *n*, number of cells analyzed.

1. MacLaren RE, et al. (2006) Retinal repair by transplantation of photoreceptor precursors. *Nature* 444(7116):203–207.

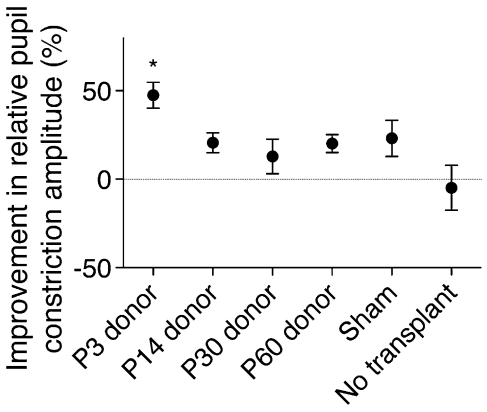

Fig. S6. Degenerate *rd1* hosts that received donor cells from P14, P30, and P60 animals did not show an improvement in relative pupil constriction amplitude over no transplant controls, whereas animals receiving P3 donor cells showed robust functional restoration ($F_{5,64} = 3.64$, $P = 0.006$, $^*P < 0.05$ post hoc versus no transplant controls; $n = 11–14$ in each group). Error bars, SE of mean.

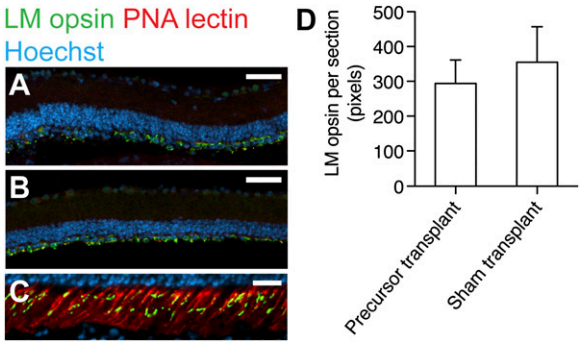

Fig. S7. Residual cone cells in precursor-treated and sham-treated eyes appear similarly abnormal. (*A* and *B*) Residual host cones, still present in the retinal periphery in both rod precursor-treated (*A*) and sham-treated (*B*) retinas, were morphologically abnormal and showed mislocalization of long/medium wavelength cone opsin (LM opsin) protein in the somata. This has been associated with poor cone function in other studies (1). (Scale bars for *A* and *B*, 50 μm.) (*C*) In the wild type, LM opsin was concentrated at the tips of the cone outer segments, the sheaths of which are marked by peanut agglutinin (PNA) lectin. (Scale bar, 20 μm.) (*D*) There was no difference in LM opsin expression, as quantified on histological sections, between precursor-treated and sham-treated eyes ($t_{10} = 0.50$, $P = 0.6$, $n = 6$ in each group).

1. Jin M, et al. (2009) The role of interphotoreceptor retinoid-binding protein on the translocation of visual retinoids and function of cone photoreceptors. *J Neurosci* 29(5):1486–1495.

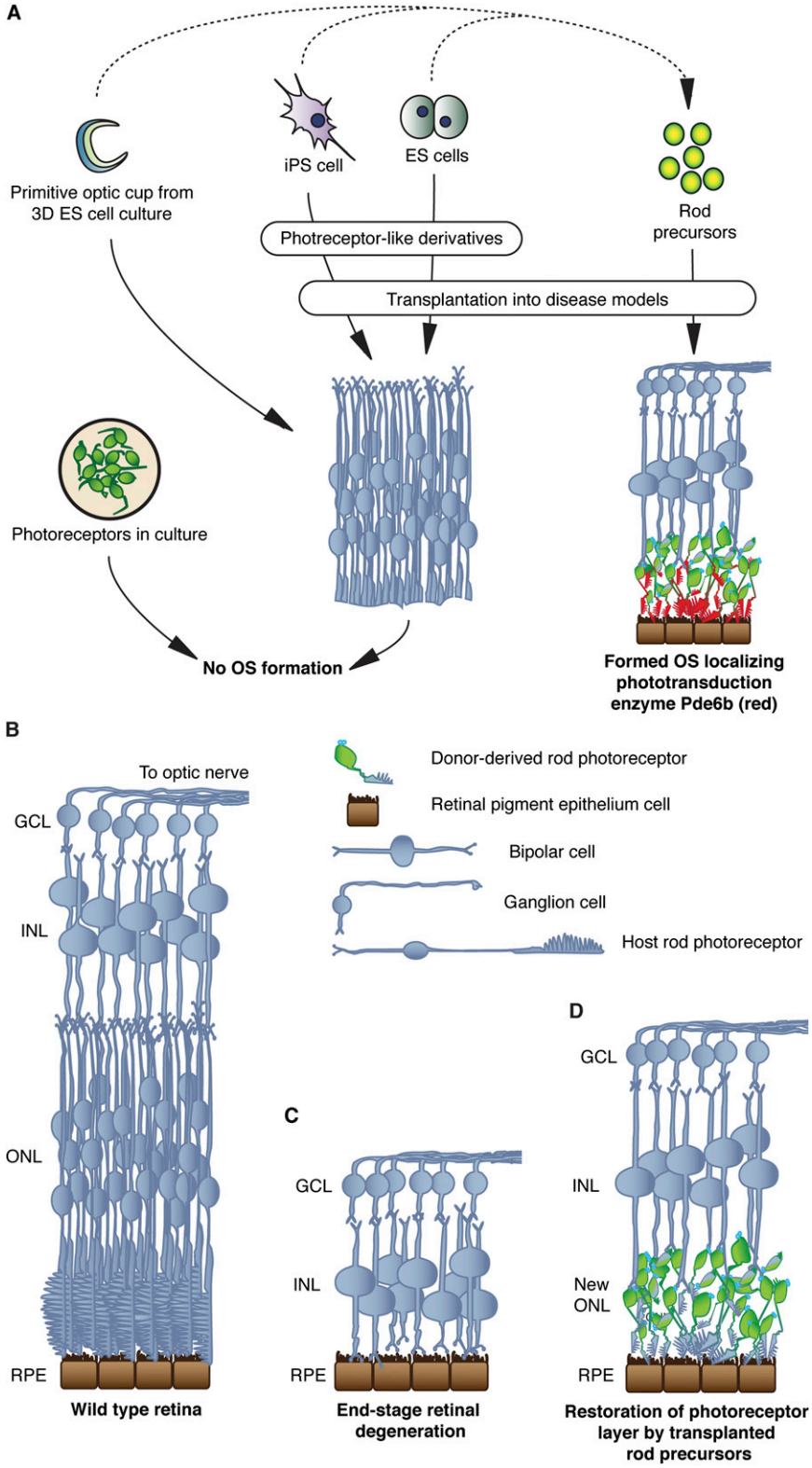

Fig. S8. Schematic illustrating that rod precursors transplanted into the adult degenerate subretinal space can generate OS. (*A*) Rod precursors are able to give rise to formed OS after transplantation. Dotted lines indicate possible pathways to increase the OS-forming capability of different renewable cell sources. (*B*) The normal trilaminar appearance of wild-type retina (for clarity, only rods, bipolar cells, and ganglion cells are shown). (*C*) In end-stage retinal degeneration, the photosensitive outer nuclear layer is lost completely. (*D*) The entire photoreceptor layer can be reconstructed when rod precursor cells (green) are transplanted into the subretinal space under optimal conditions. These cells make synaptic contacts (blue dots) with host bipolar cells in the inner nuclear layer. ES cell, embryonic stem cell; GCL, ganglion cell layer; INL, inner nuclear layer; iPS cell, induced pluripotent stem cell; ONL, outer nuclear layer; Pde6b, cGMP phosphodiesterase 6β; RPE, retinal pigment epithelium.

Table S1. Primary antibodies used for immunohistochemistry

Antibody	Source	Dilution
Rabbit anti-PDE6β	Abcam	1:1,000
Rabbit anti-synaptophysin	Abcam	1:1,000
Rabbit anti-protein kinase Cα	Epitomics	1:1,000
Rabbit anti-red/green opsin	Millipore	1:1,000
Rabbit anti-rhodopsin	Abcam	1:100
Rabbit anti-rod outer segment membrane protein1	Abcam	1:300
Rabbit anti-transducin α (GNAT1)	Abcam	1:100
Rabbit anti-recoverin	Millipore	1:1,000
Rabbit anti-bassoon	Abcam	1:1,000
Rabbit anti-ABCA4	Abcam	1:1,000
Rabbit anti-glial fibrillary acid protein	Abcam	1:1,000
Rabbit anti-peripherin 2	Proteintech	1:200
Rabbit anti-interphotoreceptor retinoid-binding protein	Santa Cruz	1:300
Lectin peanut agglutinin Alexa-488	Invitrogen	1:100

Table S2. Primers used in PCR reactions

Gene	Primer	Sequence
Pde6b	Forward	TGGAGAACCGTAAGGACATCGC
	Reverse	TCCTCACAGTCAGCAGGCTCTT
Nr2e3	Forward	GCCTTATCACCGCCGAAACTTG
	Reverse	CATGGATGCCATCCAGACTGCA
Cnga1	Forward	CGGATGGAAAATGGAGCGTGCA
	Reverse	CTCTGTGATGGTCCTCGCCTTT
Gnat1	Forward	GCTTGTGGAAGGACTCGGGTAT
	Reverse	AACGCAACACGTCCTGCTCAGT
Rho	Forward	GAGGGCTTCTTTGCCACACTTG
	Reverse	AGCGGAAGTTGCTCATCGGCTT

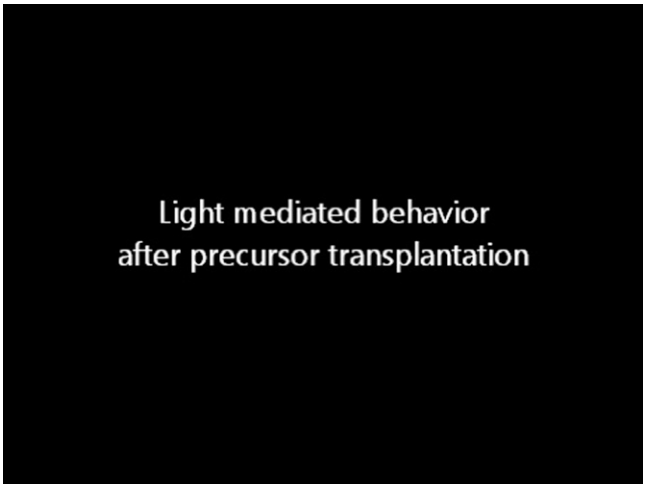

Movie S1. Light-mediated behavior after precursor cell transplantation. This *rd1* mouse had received bilateral transplants of cell suspensions obtained from P3 Tg(*Nrl-L-EGFP*) mice, 2 wk before the test. Preference for the light or dark compartment was tested under dim 510-nm light (150 nW·cm^{-2}·s^{-1}, ~10 lx). The movie is a 5-min excerpt from a 10-min trial, shown at 4× speed, and the overall brightness has been enhanced for clarity.

Movie S1

Movie S2. Light-mediated behavior after sham transplantation. This *rd1* mouse had received bilateral transplants of cell suspensions obtained from adult *rd1* mice, 2 wk before the test. Preference for the light or dark compartment was tested under dim 510-nm light (150 nW·cm^{-2}·s^{-1}, ~10 lx). The movie is a 5-min excerpt from a 10-min trial, shown at 4× speed, and the overall brightness has been enhanced for clarity.

Movie S2